

## FINITE ELEMENT ANALYSIS OF WRINKLING DURING CUP DRAWING

D.M. Neto<sup>\*</sup>, P.D. Barros<sup>\*</sup>, M.C. Oliveira<sup>\*</sup>, J.L. Alves<sup>†</sup> and L.F. Menezes<sup>\*</sup>

<sup>\*</sup> Mechanical Engineering Center from University of Coimbra (CEMUC)  
Department of Mechanical Engineering, University of Coimbra  
Polo II, Rua Luís Reis Santos, 3030-788 Coimbra, Portugal  
e-mail: {diogo.neto, pedro.barros, marta.oliveira, [luis.menezes](mailto:luis.menezes@dem.uc.pt)}@dem.uc.pt, www.uc.pt

<sup>†</sup> Center for Mechanical and Materials Technologies (CT2M)  
Department of Mechanical Engineering, University of Minho  
Campus de Azurém, Guimarães, 4800-058, Portugal  
email: [jlalves@dem.uminho.pt](mailto:jlalves@dem.uminho.pt), www.uminho.pt

**Key Words:** *Wrinkling, Finite element method, Mesh refinement, Yield criteria, DD3IMP.*

**Abstract.** This work focuses on the analysis of the NUMISHEET 2014 Benchmark 4 – Wrinkling during cup drawing, which had as objective to investigate the effects of geometry and the materials model on a dome wrinkling (puckering) behavior. Two different punch geometries were proposed and two materials were selected: an aluminum alloy, AA5042, and a mild steel, AKDQ. The mechanical behavior of both materials is described using a Voce type isotropic work-hardening law combined with two yield criteria: Hill'48 and Cazacu and Barlat 2001. The study highlights the influence of the in-plane mesh refinement and of the yield criterion adopted. The comparison between the numerical and the experimental results is presented to evaluate the effectiveness of the yield criterion selected. Following the benchmark description, the main process parameters studied are the punch force evolution and the cup radial coordinate versus the angle from rolling direction after the drawing process. The results show that accurate wrinkling prediction requires a good selection of the in-plane mesh refinement but also an accurate description of the orthotropic behavior of the material.

### 1 INTRODUCTION

Sheet metal forming is one of the manufacturing processes where the use of finite element analysis (FEA) had the largest impact in the design stage, driven by the strong demands on high precision and high value-added products imposed by sectors such as the automotive industry, aircraft industry and can industry. FEA allows reducing process development time and to obtain high precision products, since it allows the prediction of defects and design modifications at the design stage.

The major defects in sheet metal forming processes are tearing, springback and other geometric surface defects, including wrinkling. Nowadays, thin high strength sheet metals are being used on various types of automotive parts. On the other hand, the improvements on can

manufacturing technology and cost control efforts have resulted in a consistent reduction of the net metal weight and cost which led to beverage cans with thinner sidewalls, reduced neck diameters and smaller base diameters [1]. However, small diameter cans and light gauge material increases the likelihood of wrinkling during sheet metal forming. Thus, wrinkling is becoming a more prevalent failure mode. Wrinkling is a kind of local buckling of sheet metal which is formed by excessive compressive stresses, i.e. it results from instability under compressive stresses [2]. Manufacturing experience suggests that wrinkling is influenced by various factors such as mechanical properties of the aluminium sheet, tooling geometry, contact conditions including the effects of lubrication, and process boundary conditions [1]. Thus, unlike the fracture limit that can be estimated using strain or stress values, the wrinkling limit will also be highly influenced by geometry and contact conditions. In fact, the initiation and growth of wrinkles are influenced by many factors such as the stress ratio, the mechanical properties of the sheet material, the blank geometry and the contact conditions. The effects of all these factors are very complex and the studies of wrinkling behaviour may show a wide scattering of data for small deviations in factors, as is common in instability phenomena [3]. In fact, small variations of the parameters can result in widely different wrinkling behaviours [1].

The two main categories of wrinkling that may occur during deep drawing are flange and wall wrinkles [4], which are basically originated from the compressive circumferential stresses. However, wall wrinkling occurs far more easily than the wrinkling on the flat flange since the wall is relatively unsupported by the tool. Also, the suppression of wall wrinkles is more difficult than the suppression of flange wrinkles, which can be controlled by increasing the blank holder force, i.e. by changing the radial tensile stress component [2]. However, in order to improve the productivity and the quality of products, wrinkling must be suppressed.

## 2 DRAWING OF A CYLINDRICAL CUP

This work focuses on the analysis of the NUMISHEET 2014 Benchmark 4 – Wrinkling during cup drawing, which had as objective to investigate the effects of geometry and the materials model on a dome wrinkling (puckering) behaviour [1]. Two different punch geometries were proposed and two materials were selected: an aluminium alloy, AA5042, and a mild steel, AKDQ. Figure 1 presents an example of draw cylindrical cup with occurrence of wrinkles in the wall.



**Figure 1:** Draw cup with wrinkles [1].

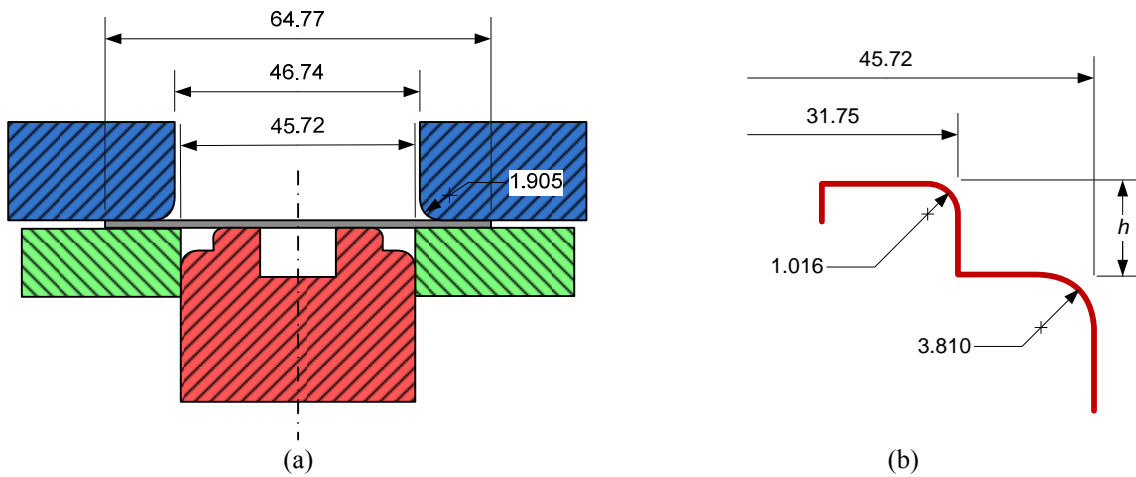


**Figure 2:** Schematic view of tools and their dimensions (mm) for the: (a) drawing process; (b) detail view of the punch.

Figure 2 presents a schematic view of tools used in the drawing process, as well as their principal dimensions in millimetres. As mentioned before, two different punch geometries are employed, being the dimension  $h$  shown in Figure 2 (b), the only difference between them. The dimension  $h$  is higher in punch A than in punch C, being defined as  $h=5.207$  mm and  $h=3.429$  mm, in the punch A and punch C, respectively. The circular blank considered for this benchmark has 64.77 mm diameter and 0.2083 mm of initial thickness for the AA5042 aluminium alloy, while the initial thickness for the AKDQ mild steel is 0.2235 mm. The blank holder force has a constant value of 8.9 kN and the total punch stroke considered is 18 mm (the cup is completely drawn).

## 2.1 Numerical model

The numerical simulations were performed with DD3IMP in-house code, which is a fully implicit solver that has been developed to simulate sheet metal forming processes [5, 6]. The forming tools are considered as rigid and its surface is defined with Nagata patches [7], being the required normal vectors for the surface smoothing evaluated using the algorithm proposed in [8]. The contact conditions are described by the Coulomb's law, being the friction coefficient between sheet and tools taken from the benchmark specifications as  $\mu=0.03$ . The mechanical behaviour of both materials is described using a Voce type isotropic work hardening law, being the parameters indicated in Table 1. The elastic proprieties of both materials are also indicated in the same table [1].

Concerning the yield criteria employed to describe the material anisotropic behaviour, two yield functions are considered in this study: Hill'48 and Cazacu and Barlat 2001 (CB'01) [9]. The yield parameters identification procedure adopted is based on the minimization of an error function that evaluates the difference between the estimated values and the experimental ones. Table 2 presents a summary of the parameters obtained, for both materials and yield criteria. Since in metallic sheets it is not possible evaluate the  $a_5$ ,  $a_6$ ,  $b_6$ ,  $b_7$ ,  $b_8$ ,  $b_9$  and  $b_{11}$  parameters of the CB'01, the values considered are the ones used for isotropy, i.e. 1.0 [10, 11].

**Table 1:** Elastic proprieties and parameters of the work hardening rule (Voce law) for both materials studied [1].

	$E$ [GPa]	$\nu$	$Y_0$ [MPa]	$Y_{sat}$ [MPa]	$C$
AA5042	68.9	0.33	267.8	375.1	17.86
AKDQ	210.0	0.30	297.8	471.8	15.89

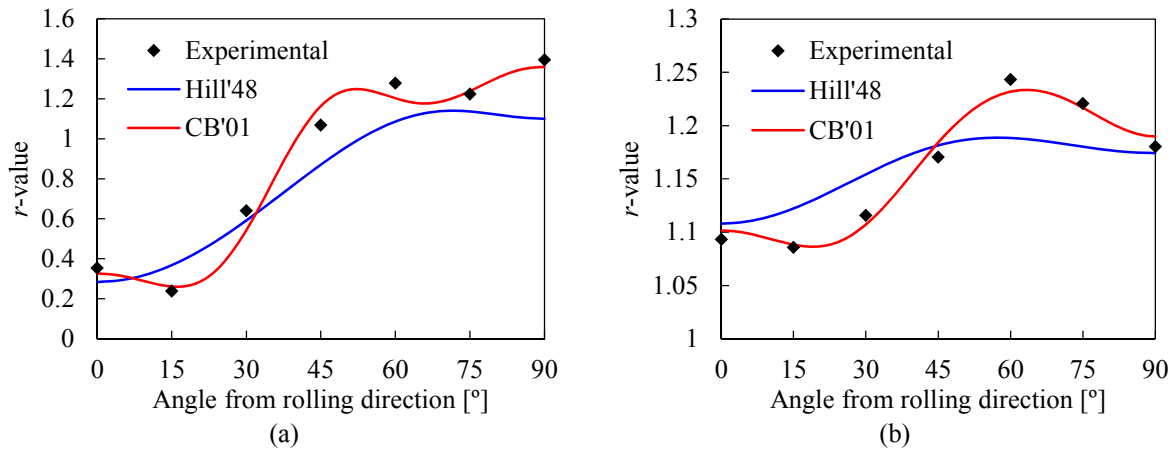
**Table 2:** Material parameters of the yield criteria defined for both materials studied.

	Hill'48				
	$F$	$G$	$H$	$N$	$L=M$
AA5042	0.246	0.955	0.270	1.646	1.500
AKDQ	0.403	0.427	0.473	1.395	1.500

	Cazacu and Barlat (CB'01)										
	$a_1$	$a_2$	$a_3$	$a_4$	$b_1$	$b_2$	$b_3$	$b_4$	$b_5$	$b_{10}$	$c$
AA5042	0.838	0.981	1.242	1.252	37.49	9.458	31.94	8.142	-18.08	15.89	0.004
AKDQ	1.050	0.957	0.968	1.056	1.173	1.118	1.168	1.075	0.884	1.051	1.710

Figure 3 presents the comparison between experimental and predicted  $r$ -values for both AA5042 aluminium alloy and AKDQ steel. For both materials analysed, the experimental  $r$ -values are better predicted using the CB'01 yield criterion than using the classical Hill'48 yield criterion. Note that the AKDQ material is only slightly anisotropic (see  $r$ -values range Figure 3 (b)), while the experimental  $r$ -values of the aluminium alloy ranges from 0.2 to 1.4, as shown in Figure 3 (a). Regarding the yield stress evolution in the sheet plane, both materials present only slight anisotropy.

**Figure 3:** Comparison between experimental and predicted  $r$ -values for: (a) aluminum alloy AA5042; (b) AKDQ steel.

### 3 FINITE ELEMENT MESH SENSITIVITY ANALYSIS

The numerical model adopted in this study considers only one quarter of the model due to geometric and material symmetry conditions. The circular blank is discretized with 8-node

hexahedron solid finite elements, allowing the accurate evaluation of the contact forces through an accurate description of contact evolution and thickness change. The in-plane mesh refinement of the blank has been identified as a numerical parameter that strongly influences the wrinkling prediction [3]. Thus, the influence of mesh refinement is analysed using different blank discretizations. In order to build a structured mesh in the area with potential wrinkling occurrence, the blank geometry is divided in two zones, as shown in Figure 4. The central zone (radius inferior to 12.5 mm), which is the flat part of the punch (see Figure 2) is characterized by small strains during all process. Thus, it is defined by a relatively coarse unstructured mesh. On the other hand, the blank area with potential wrinkling occurrence is discretized with a fine structured mesh in order to accurately reproduce the wrinkling waves.

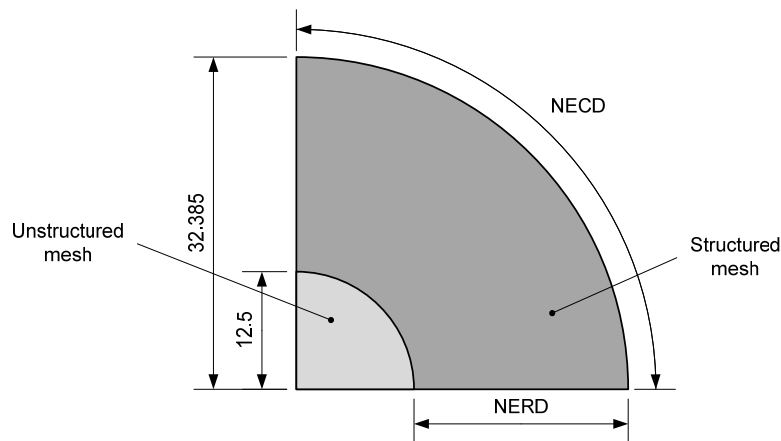


**Figure 4:** Division of the blank in two zones to perform a structured mesh on the important region.

Three different finite element meshes are studied and compared, all using 2 layers of elements through the thickness. Table 3 presents the number of hexahedron solid finite elements used in each mesh. Concerning the structured mesh region (see Figure 4), both the number of elements in the radial direction (NERD) and the number of elements in the circumferential direction (NECD) are specified in Table 3, for each mesh analyzed. The number of finite elements employed in each region (structured and unstructured) is indicated, as well the total number of hexahedron finite elements adopted in the numerical model to discretize the blank.

**Table 3:** Number of solid finite elements employed in each zone of the blank for three different meshes.

	NERD	NECD	Structured mesh	Unstructured mesh	Total of solid elements
Mesh #1	100	100	20000	2546	22546
Mesh #2	120	200	48000	3802	51802
Mesh #3	150	250	75000	4630	79630

In order to analyze the influence of the yield criterion adopted on the finite element mesh selection, the sensitivity finite element analysis is performed for both isotropic (von Mises)

and anisotropic (CB'01) material behavior. This analysis is carried out using the aluminum alloy AA5042 since it is much more anisotropic than the AKDQ, as shown in Figure 3. Moreover, the punch A is the condition adopted because the distance  $h$  is higher (see Figure 2 (a)), which increases the likelihood of wrinkling occurrence. All numerical simulations are carried on a computer machine equipped with an Intel® Core™ i7–2600 K Quad-Core processor (3.4 GHz) and the Windows 7 Professional (64-bits platform) operating system.

### 3.1 Isotropic material

The three finite element meshes presented in Table 3 are employed in the numerical simulation of the cup drawing. The punch force evolution with its displacement is shown in Figure 5 (a) for each mesh. Since all meshes are structured in the region of contact with the tools, each entirely line of nodes in the circumferential direction comes into contact with the tool at the same time for a material with isotropic behavior. Thus, small oscillations in the punch force evolution occur, particularly for the coarse mesh (mesh #1), which presents a smaller value for the NERD parameter. The cup radial coordinate versus the angle from rolling direction after the drawing process, at the plane  $z=-4.5$  mm (origin is on the top surface of the drawn cup), is presented in Figure 5 (b) for each mesh analyzed. For both results evaluated, only mesh #1 leads to significant differences, as shown in Figure 5. Indeed, the number of elements used in mesh #1 (see NECD in Table 3) is not sufficient to reproduce accurately the wrinkling waves, including the instant they contact with the punch.

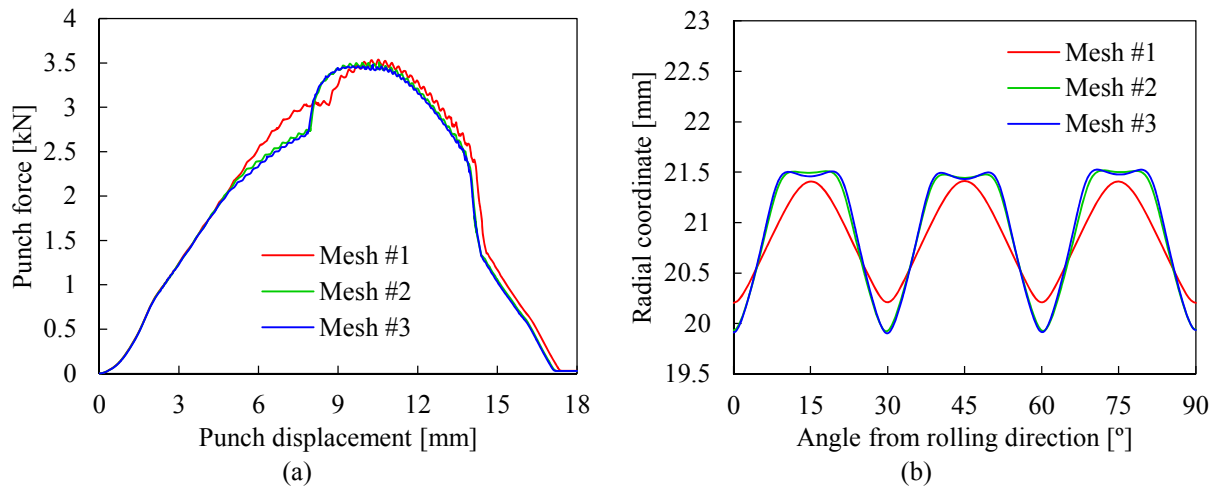


**Figure 5:** Influence of the finite element mesh adopting the von Mises yield criterion (AA5042 and punch A): (a) punch force evolution; (b) radial coordinate as function of the angle with the rolling direction.

**Table 4:** Number of increments and CPU time for three different discretizations, adopting the von Mises yield criterion (AA5042 and punch A).

	Mesh #1	Mesh #2	Mesh #3
N° of increments	706	725	748
CPU time [h]	6.4	22.7	69.8

Table 4 contains the computational performance obtained with each finite element mesh. The number of increments required to complete the forming process is between 706 and 748 for the coarser and finer mesh, respectively. On the other hand, the CPU time increases exponentially with the mesh refinement, as shown in Table 4. In fact, the computational time required to carry out the simulation using the finer mesh (mesh #3) is about 3 days, while the adoption of mesh #2 leads a computational time inferior to 1 day.

### 3.2 Anisotropic material

This section contains the finite element sensitivity analysis using the CB'01 yield criterion to describe the material anisotropic behavior. Figure 6 (a) presents the punch force evolution with its displacement for each mesh studied. As for the isotropic material behavior, only mesh #1 leads to significant differences in the force evolution (see Figure 5 (a)). The cup radial coordinate as function of the angle from rolling direction, at the plane  $z=-4.5$  mm, is shown in Figure 6 (b) for each mesh. As oppose to the isotropic material behavior, slightly differences in the radial coordinate can be observed between mesh #2 and mesh #3, which occurs closer to the rolling direction. The anisotropic material behavior (see Figure 3 (a)) leads to a non-uniform distribution of the blank holding force. In this case, closer to the rolling direction the  $r$ -values are smaller than 1.0 while closer to the transverse direction they are higher. This leads to inferior restraining forces closer to the rolling direction, being the numerically predicted values more sensitivity to the mesh refinement adopted. Also, the sheet can freely produce more wrinkling waves in this area, but this effect can only be predicted if the finite element mesh adopted is sufficiently refined.

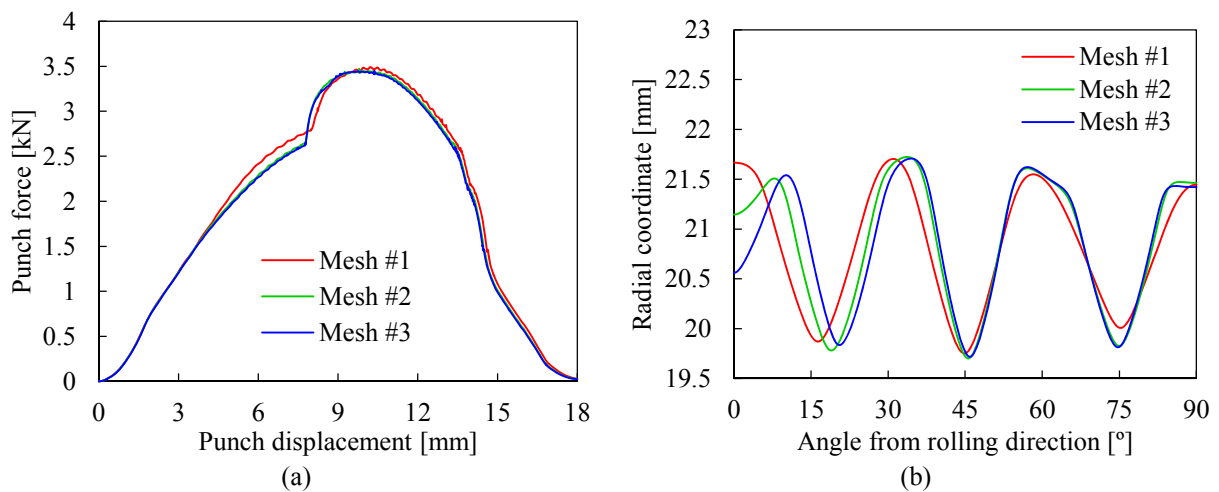


**Figure 6:** Influence of the finite element mesh adopting the CB'01 yield criterion (AA5042 and punch A): (a) punch force evolution; (b) radial coordinate as function of the angle with the rolling direction.

Both the number of increments and the CPU time follow the same trend observed for the isotropic material (compare Table 4 and Table 5). However, globally the required CPU time is slightly inferior in this case because the numerical instabilities related with the isotropic material behavior (isotropic mesh of the blank in axisymmetric problems) are eliminated. Note that the oscillations in the punch force are also eliminated or significantly reduced.

Taking into account the computational time and the accuracy of the numerical results obtained, mesh #2 is adopted in the following analysis.

**Table 5:** Number of increments and CPU time for three different discretizations, adopting the CB'01 yield criterion (AA5042 and punch A).

	Mesh #1	Mesh #2	Mesh #3
N° of increments	684	717	716
CPU time [h]	5.3	20.7	50.5

## 4 RESULTS AND DISCUSSION

The comparison between the numerical results and the experimental ones is presented to evaluate the effectiveness of the yield criterion selected as well as the finite element mesh adopted (mesh #2). The main process parameters studied are the punch force evolution and the cup radial coordinate versus the angle from rolling direction after the drawing process, evaluated in the plane at  $z=-4.5$  mm.

### 4.1 Aluminum alloy AA5042

The comparison between experimental and numerically predicted punch force evolution for the aluminum alloy AA5042, using both the punch A and the punch C is presented in Figure 7 (a) and (b), respectively. For each process condition, the experimental tests were run in triplicate by the benchmark committee, being only one presented in this study [1]. The experimental punch force is overestimated by the numerical model for both conditions (punch A and punch C) independently of the yield criteria selected (Hill'48 and CB'01). Globally, the punch force predicted by the Hill'48 yield criterion is slightly higher than the one obtained with the CB'01 criterion, as shown in Figure 7. The instant (punch displacement) for which the punch force increase abruptly, due to contact of the wrinkles with the punch, is well predicted in both models. Moreover, the punch displacement for which the blank lost contact with the blank-holder is also accurately predicted (approximately 14.5 mm), as well the punch force evolution after this instant.

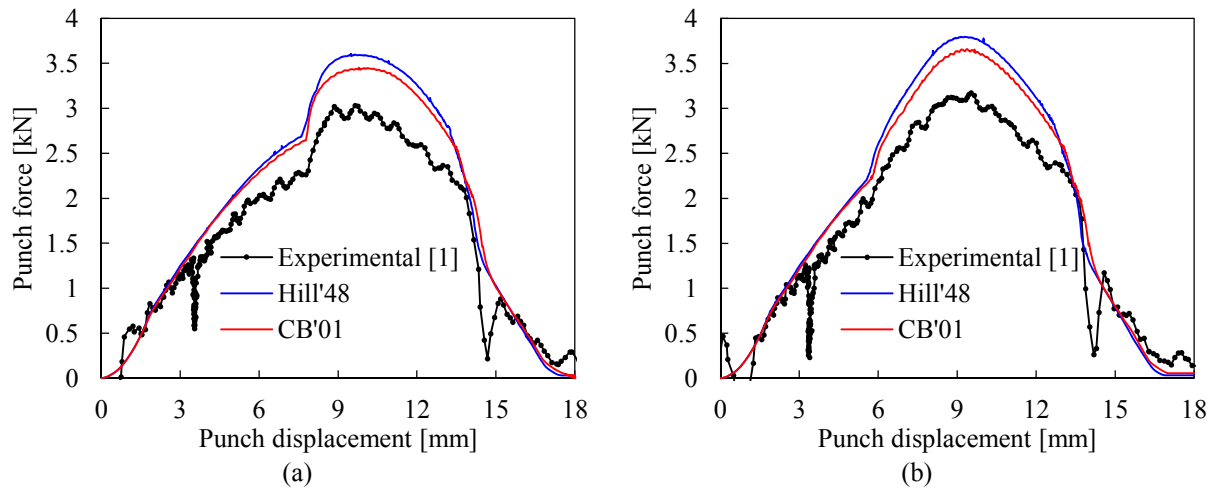


**Figure 7:** Comparison between predicted and experimental punch force evolution (AA5042): (a) punch A; (b) punch C. Note that there is a small misprint in the conference proceedings [1] concerning the experimental punch force evolution for punch A.

Figure 8 presents the comparison between experimental and numerical cup radial coordinate evaluated in the plane at  $z=-4.5$  mm after the drawing process using punch A. The number of the wrinkling waves observed experimentally is 13, which is between the 12 predicted by the model using the CB'01 yield criterion and the 14 predicted with the Hill'48 criterion. The amplitude of the waves is approximately the same in both yield criteria and is in good agreement with experimental observations. Nevertheless, the shape of the waves obtained with the CB'01 yield criterion is closer to the one observed experimentally, as shown in Figure 8. The comparison between experimental and numerical cup radial coordinate evaluated in the plane at  $z=-4.5$  mm after the drawing process using punch C is shown in Figure 9. The shape of the wrinkling waves is completely different from the one obtained with punch A, but the number of waves is the same, both experimentally and numerically. The shape of the waves is accurately predicted, nevertheless its amplitude is slightly inferior in the numerical model. The Hill'48 yield criterion does not predicts wrinkles closer to the rolling direction, while the CB'01 criterion predicts small wrinkling waves in the transverse direction, as shown in Figure 9.

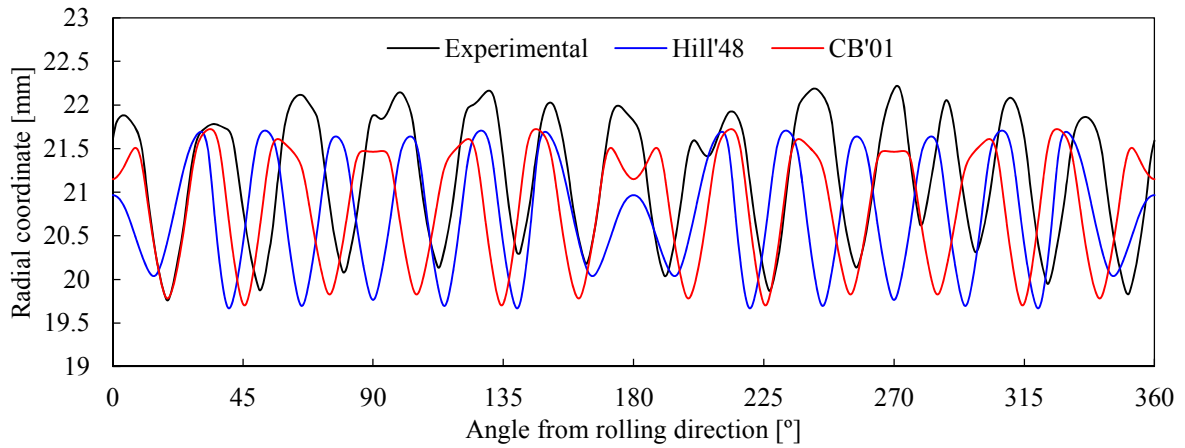


**Figure 8:** Cup radial coordinate ( $z=-4.5$  mm) as function of the angle from rolling direction after the drawing process (AA5042) using punch A.

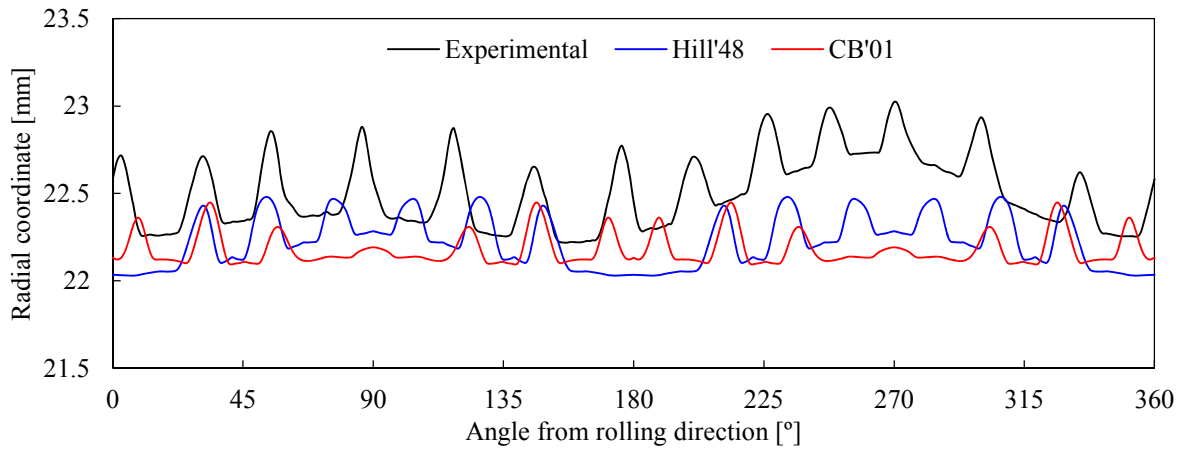


**Figure 9:** Cup radial coordinate ( $z=-4.5$  mm) as function of the angle from rolling direction after the drawing process (AA5042) using punch C.

## 4.2 AKDQ steel

The comparison between experimental and numerically predicted punch force evolution for the AKDQ steel is presented in Figure 10 (a) and (b) for the punch A and the punch C, respectively. The experimental punch force is underestimated by the numerical model for both conditions (punch A and punch C) and for both yield criteria selected (Hill'48 and CB'01). Indeed, the punch force is accurately predicted until the instant that the force increases abruptly due to the contact of the punch with the wrinkles. The punch displacement for which this occurs is incorrectly predicted for the punch A (see Figure 10 (a)), while in the process conditions with punch C this instant is properly predicted (see Figure 10 (b)). Moreover, the abrupt decrease in the punch force dictated by the lost contact between blank and blank-holder is accurately predicted, as well as the following trend.

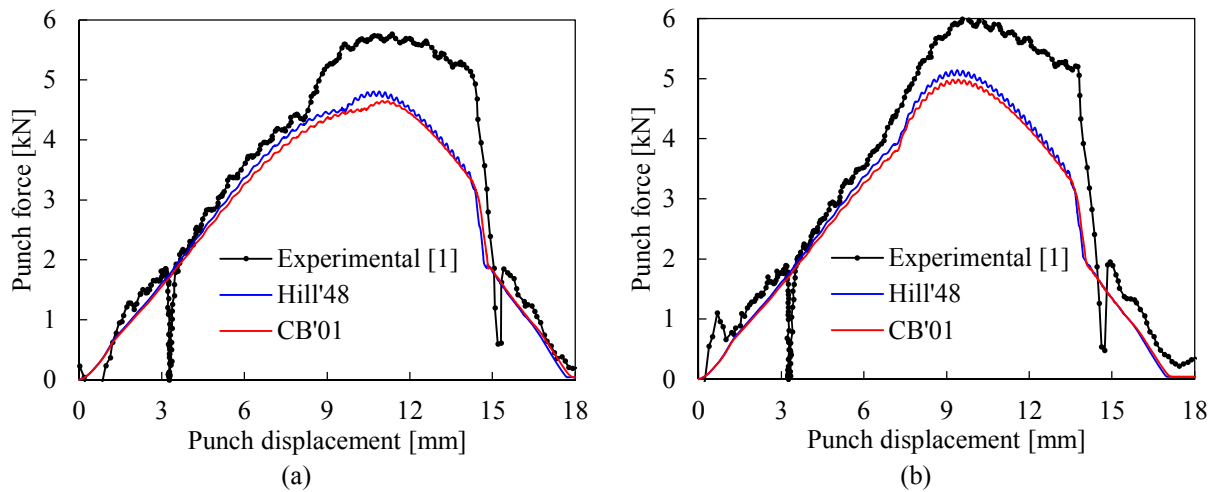


**Figure 10:** Comparison between predicted and experimental punch force evolution (AKDQ): (a) punch A; (b) punch C.

The comparison between experimental and numerical cup radial coordinate evaluated in the plane at  $z=-4.5$  mm, after the drawing process, using punch A is shown in Figure 11. The amplitude of the wrinkling waves is clearly underestimated by both yield criteria. The numerical results obtained with the Hill'48 yield criterion are closer to the experimental ones. These results are in accordance with the punch displacement for which the contact between wrinkling waves and punch occurs, since this is better predicted by the Hill'48 yield criterion (see Figure 10 (a)). The number of waves predicted by the CB'01 yield criterion is 10, while the Hill'48 criterion leads a cup with 12 waves, being 11 the number of waves observed experimentally. Figure 12 presents the comparison between experimental and numerical cup radial coordinate evaluated in the plane at  $z=-4.5$  mm, after the drawing process using punch C. Globally, no wrinkling occurrence is predicted by both numerical models, while in the experimental result only small oscillations in the radial coordinate are observed. The difference between experimental and numerical radial coordinate is approximately 0.25 mm, being the experimental radial coordinate underestimated by the numerical models.

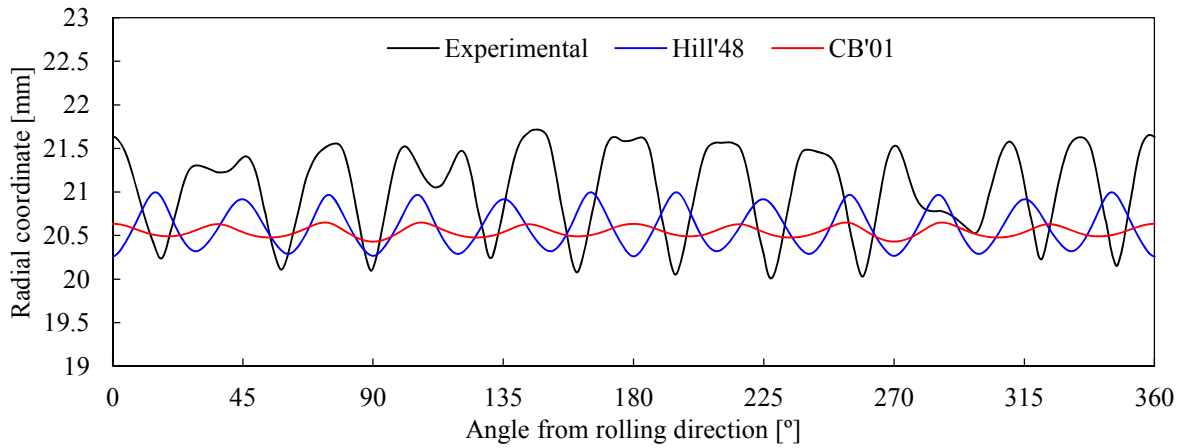


**Figure 11:** Cup radial coordinate ( $z=-4.5$  mm) as function of the angle from rolling direction after the drawing process (AKDQ) using punch A.

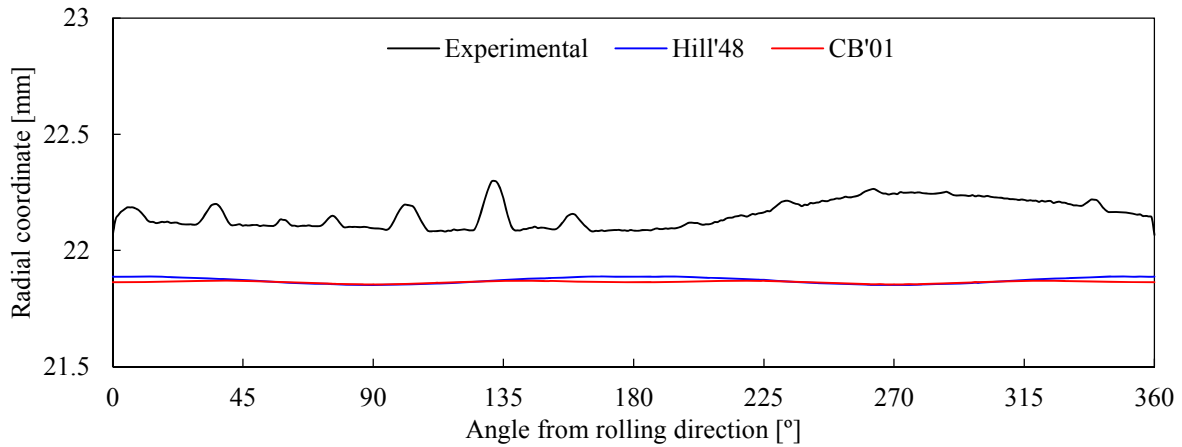


**Figure 12:** Cup radial coordinate ( $z=-4.5$  mm) as function of the angle from rolling direction after the drawing process (AKDQ) using punch C.

## 5 CONCLUSIONS

This study deals with the prediction of wrinkling during the cup drawing using the finite element analysis. The selected example is the one proposed as benchmark in the NUMISHEET 2014 conference. Two different punch geometries are compared for each material analysed (AA5042 and AKDQ steel). For both materials, the anisotropic material behavior is described by two yield criteria: Hill 1948 and Cazacu and Barlat 2001. The finite element mesh sensitivity analysis shows that accurate wrinkling waves prediction requires a correct selection of the finite element mesh for the blank. Thus, the selected mesh must be finer than the one typically employed in the drawing process without wrinkles. Moreover, the anisotropic behavior of the material dictates more complex frictional contact conditions with the blank-holder, which increases the need for an even finer mesh. The presented numerical results are in good agreement with the experimental ones, both in terms of punch force evolution and in the occurrence of wrinkling. Indeed, the shape, amplitude and number of

wrinkling waves are accurately predicted using a fine mesh and an appropriate constitutive law for the material behavior, particularly for the aluminum alloy.

## ACKNOWLEDGEMENTS

This research work is sponsored by national funds from the Portuguese Foundation for Science and Technology (FCT) via the projects PTDC/EMS-TEC/1805/2012 and PEst-C/EME/UI0285/2013 and by FEDER funds through the program COMPETE – Programa Operacional Factores de Competitividade, under the project CENTRO -07-0224 -FEDER - 002001 (MT4MOBI). The first author is also grateful to the FCT for the PhD grant SFRH/BD/69140/2010.

## REFERENCES

- [1] Dick, R., Cardoso, R., Paulino, M. and Yoon, J.W. Benchmark 4 - Wrinkling during cup drawing. *AIP Conf. Proc* (2013) **1567**:262-327.
- [2] Shafaat, M.A., Abbasi, M. and Ketabchi, M. Investigation into wall wrinkling in deep drawing process of conical cups. *J. Mater. Process. Tech* (2011) **211**:1783-1795.
- [3] Kim, J.B., Yoon, J.W. and Yang, D.Y. Investigation into the wrinkling behaviour of thin sheets in the cylindrical cup deep drawing process using bifurcation theory. *Int. J. Numer. Meth. Engng* (2003) **56**:1673-1705.
- [4] Wang, C.T., Kinzel, G. and Altan, T. Wrinkling criterion for an anisotropic shell with compound curvatures in sheet forming. *Int. J. Mech. Sci* (1994) **36**:945-960.
- [5] Menezes, L.F. and Teodosiu, C., Three-dimensional numerical simulation of the deep-drawing process using solid finite elements. *J. Mater. Process. Tech* (2000) **97**:100-106.
- [6] Menezes, L.F., Neto, D.M., Oliveira, M.C. and Alves, J.L. Improving computational performance through HPC techniques: case study using DD3IMP in-house code. *AIP Conf. Proc* (2011) **1353**:1220-1225.
- [7] Neto, D.M., Oliveira, M.C., Menezes, L.F. and Alves, J.L. Applying Nagata patches to smooth discretized surfaces used in 3D frictional contact problems. *Comput. Methods Appl. Mech. Engng* (2014) **271**:296-320.
- [8] Neto, D.M., Oliveira, M.C., Menezes, L.F. and Alves, J.L. Nagata patch interpolation using surface normal vectors evaluated from the IGES file. *Finite Elem. Anal. Des* (2013) **72**:35-46.
- [9] Cazacu, O., Barlat, F. Generalization of Drucker's yield criterion to orthotropy. *Math. Mech. Solids* (2001) **6**:613-630.
- [10] Barros, P.D., Simoes, V.S., Neto, D.M., Oliveira, M.C., Alves, J.L. and Menezes, L.F. On the influence of the yield parameters identification procedure in cylindrical cups earing prediction. *AIP Conf. Proc* (2013) **1567**:512-515.
- [11] Barros, P.D., Oliveira, M.C., Alves, J.L. and Menezes, L.F. Earing prediction in drawing and ironing processes using an advanced yield criterion. *Key Eng. Mater* (2013) **554-557**:2266-2276.